10.1071/ES21015
Journal of Southern Hemisphere Earth Systems Science

Supplementary Material

The Antarctic ozone hole during 2020

Andrew R. Klekociuk[A,*], *Matthew B. Tully*[B], *Paul B. Krummel*[C], *Stuart I. Henderson*[D], *Dan Smale*[E], *Richard Querel*[E], *Sylvia Nichol*[F], *Simon P. Alexander*[A], *Paul J. Fraser*[C] and *Gerald Nedoluha*[G]

[A]Australian Antarctic Division, Department of Agriculture, Water and the Environment, Kingston, Tas., Australia.

[B]Bureau of Meteorology, Melbourne, Vic., Australia.

[C]Climate Science Centre, CSIRO Oceans and Atmosphere, Aspendale, Vic., Australia.

[D]Australian Radiation Protection and Nuclear Safety Agency, Yallambie, Vic., Australia.

[E]National Institute of Water & Atmospheric Research, Lauder, New Zealand.

[F]National Institute of Water & Atmospheric Research, Wellington, New Zealand.

[G]Naval Research Laboratory, Washington, DC, USA.

*Correspondence to: Email: andrew.klekociuk@awe.gov.au

1. In situ measurements and ground-based remote sensing

Figure S1 shows total column observations by the Dobson spectrophotometer at Arrival Heights, which provide additional detail to the measurements presented in Fig. 3a. Figure S1 includes observations during the polar night using the moon as a reference source.

Figure S2 compares partial column ozone values over the 14-22 km altitude range from ozonesonde measurements in 2020 with all available earlier years at Davis (Fig. S2a), Macquarie Island (Fig. S2b) and Broadmeadows (Fig. S2c). A notable feature of the Davis measurements in 2020 was that some values from late-October to mid-December (day-of-year 300-350) were climatologically below or near the smallest observed since measurements began in 2003 (with minimum values of 19 DU on 4 November and 18 DU on 11 November) and similar to values seen in

spring in some years with the strongest ozone loss (such as 2006 and 2015). Figure S2b indicates that the partial column values at Macquarie Island on some occasions between days 275 to 325 (approximately spanning October to mid-November) in 2020 were at or near the lowest values observed for that time of year. While Macquarie Island is normally well-equatorward of the polar vortex edge (Fig. 1), these low values indicate that there was weak ozone accumulation in the mid-latitude stratospheric ridge at the time. Further north at Broadmeadows (Fig. S2c), some measurements in spring and early-summer were also relatively low compared with other years of the record.

2. Stratospheric conditions

Figure S3 presents the pressure-time section of standardised temperature anomalies over the Antarctic polar cap in 2020. Figure S3 shows that significant descending stratospheric cold and warm temperature anomalies occurred in the polar cap towards the end of 2020, with absolute values that exceeded 4 standard deviations in November and December.

Figure S4 shows latitude-time cross-sections at 50 hPa in 2020 for temperature, zonal wind speed and geopotential height. A feature of the temperature panel (Fig. S4a) is the extent of significant cold anomalies (magenta single hatching) and new extreme low values over the climatological period that extended across all latitudes from late September. Additionally, generally low temperatures occurred at earlier times in the lower latitudes (equatorward of 45º S) and near the inner edge of the polar vortex (60º S - 80º S). The zonal wind panel (Fig. S4b) shows anomalously weak westerly winds (magenta hatched positive values) at the lower latitudes from late June through to late-September, with poleward extension from mid-August. A feature of the latter part of the year was the enhanced westerlies at the higher latitudes (black hatching), and the stronger easterlies at the lower latitudes in December. The strongest zonal winds (55º S - 65º S) were enhanced at various times (black hatching) throughout the period shown. For geopotential height, anomalously low values (magenta hatching) occurred at the extratropical latitudes, particularly from September, while in the lower latitudes, anomalous high values (black hatching) mainly occurred from late October.

Figure S5 shows the pressure-time cross section of heat flux from ERA5 data. The heat flux in the upper levels in the polar cap region during September and October 2020 was strongly supressed (blue colours). This followed a brief period of enhanced poleward heat transport in mid-August to early-September (noted in relation to Fig. 5). Poleward heat transport was also enhanced over the region in November and December relative to the climatological mean, primarily because of the late warming of the polar cap due to the persistence of the vortex.

The panels in Fig. S6 show the longitudinal variation of the mean meridional component of horizontal wave activity flux averaged over September to November for 2019 and 2020 compared with the climatology, for the lower and upper troposphere (700 hPa and 200 hPa, respectively) and in sub-polar and sub-mid-latitudes (centred on 55º S and 35º S). Negative (positive) values indicate poleward (equatorward) propagation of Rossby wave flux. The wave activity for 2020 (blue lines) was mostly within the interquartile range. However in 2019 there was strong poleward wave flux in the eastern longitudes which likely relates to the influence of the prevailing strong positive Indian Ocean Dipole (IOD) that year (Milinevsky *et al.* 2020; Rao *et al.* 2020). In contrast to 2019, tropical large-scale climate modes were generally weak in the second half of 2020, and the wave flux tended to be more strongly equatorward in the mid-latitudes during spring at 200 hPa (Fig. S6d). The La Niña phase of the El Niño Southern Oscillation (ENSO) was beginning to develop in the Pacific Ocean during September 2020, while the IOD was in a neutral to weakly negative phase (BoM, 2020).

Figure S7 shows the pressure-time cross section of the Southern Annular Mode index from empirical orthogonal function analysis of ERA5 data, highlighting the contrast between conditions in 2019 and 2020.

Figure S8a shows annual values of the S-T coupled mode index developed by Lim *et al.* (2018) to examine the situation in 2020, which, as noted in Section 3.3, strongly contrasted with conditions in 2019 in having a strong and persistent vortex. The index was obtained from area-weighted ERA5 zonal wind data gridded at 2.5º resolution, and evaluated from 1950, noting that the reanalysis is less reliable in the period before global satellite coverage began in 1979 (Hersbach *et al.* 2020). Following Lim *et al.* (2018), we define strong vortex conditions as occurring when the index is

≤ -0.8 standard deviations (σ; evaluated with respect to the 1979-2016 base period), and weak vortex conditions when the index is ≥ 0.8 σ. Over 1979 - 2020 (42 years), strong vortex conditions are indicated for the following years (σ values in parentheses; 11 years): 1987 (-1.75), 1998 (-1.07), 1999 (-1.29), 2001 (-1.36), 2006 (-0.97), 2008 (-0.81), 2010 (-1.00), 2011 (-1.03), 2015 (-1.92), 2018 (-0.96) and 2020 (-1.63). The weak vortex years are (index ≥ 0.8 σ, 9 years): 1979 (+0.89), 1988 (+1.52), 2000 (+1.04), 2002 (+2.54), 2005 (+1.00), 2012 (+1.35), 2013 (+1.27), 2016 (+1.00), and 2019 (+2.52). Our values differ slightly to Lim *et al.* (2018), which may reflect the particular reanalysis version and gridding used, although there is very good agreement overall. The strong vortex years are amongst the latest in terms of ozone hole breakdown date shown in Table 1 (Metric 8), occurring about 1 month after that for the weak vortex years.

Of the 11 strong vortex years listed above, the majority (7) were associated with the westerly QBO phase at 50 hPa during late-winter and spring, with the exceptions being 1987, 1998, 2001 and 2018 which had an easterly phase (NOAA 2021a). In 1987, the easterly QBO was weakening towards the westerly phase. The years 1998, 2001 and 2018 had persistent easterly phases, and feature in the top six in terms of strong vortex years. Note that the westerly phase of the QBO is not a necessary condition for a strong polar vortex; a westerly phase also occurred in 1988, 2002 and 2019 when the vortex was anomalously weak. Overall, the exceptions noted here highlight that the behaviour of the QBO in 2020 does not provide a strong indication as to why the polar vortex was anomalously strong in the latter part of the year.

While 2020 ranks third in terms of vortex strength (with 2015 strongest, and 1987 second strongest), the inter-annual difference in the coupled mode index between 2019 and 2020 has the largest absolute magnitude in the period since 1979 (+2.52 to -1.63 σ), as well as the greatest transition between adjacent weak and strong vortex years (Fig. S8b). As discussed by Lim *et al.* (2018), there is significant link between the SAM and ENSO in spring-summer. In particular, positive SAM conditions are favoured under the La Niña phase of ENSO. From examination of the Southern Oscillation Index (SOI) using NOAA (2021b), there is a tendency for La Niña conditions to accompany strong vortex years during the spring-summer period. Over 1979 – 2020, 7 years showed

La Niña conditions (SOI ≥ 0.7), 3 years had El Niño conditions (1987, 2006 and 2015; SOI ≤ -0.7), and 1 year (2001) showed mixed conditions. La Niña conditions in spring-summer favours the occurrence of a positive state of the tropospheric SAM, which is generally accompanied by cooler conditions in Antarctica and a southward shift of precipitation a mid-latitudes (Lim and Hendon 2015). Note that La Niña conditions are not a necessary condition for a strong vortex. Of the three most anomalously weak vortex years, 2002 and 2019 had prevailing El Niño conditions, whereas La Niña conditions occurred in 1988.

References

BoM (Bureau of Meteorology) (2020) 'La Niña underway in the tropical Pacific.' Available at http://www.bom.gov.au/climate/enso/wrap-up/archive/20200929.archive.shtml [Accessed 14 May 2021].

Hersbach, H., Bell, B., Berrisford, P., Hirahara, S., Horányi, A., Muñoz-Sabater, J., Nicolas, J., Peubey, C., Radu, R., Schepers, D., Simmons, A., Soci, C., Abdalla, S., Abellan, X., Balsamo, G., Bechtold, P., Biavati, G., Bidlot, J., Bonavita, M., De Chiara, G., Dahlgren, P., Dee, D., Diamantakis, M., Dragani, R., Flemming, J., Forbes, R., Fuentes, M., Geer, A., Haimberger, L., Healy, S., Hogan, R. J., Hólm, E., Janisková, M., Keeley, S., Laloyaux, P., Lopez, P., Lupu, C., Radnoti, G., de Rosnay, P., Rozum, I., Vamborg, F., Villaume, S., Thépaut, J.-N. (2020) The ERA5 global reanalysis. *Quarterly Journal of the Royal Meteorological Society* **146**, 1999-2049.

Lim, E.-P., Hendon, H. H. (2015) Understanding and predicting the strong Southern Annular Mode and its impact on the record wet east Australian spring 2010. *Climate Dynamics* **44**, 2807-2824.

Lim, E. P., Hendon, H. H., Thompson, D. W. J. (2018) Seasonal Evolution of Stratosphere-Troposphere Coupling in the Southern Hemisphere and Implications for the Predictability of Surface Climate. *Journal of Geophysical Research: Atmospheres* **123**, 12,002-12,016.

Milinevsky, G., Evtushevsky, O., Klekociuk, A., Wang, Y., Grytsai, A., Shulga, V., Ivaniha, O. (2020) Early indications of anomalous behaviour in the 2019 spring ozone hole over Antarctica. *International Journal of Remote Sensing* **41**, 7530-7540.

NOAA (National Oceanic and Atmospheric Administration) (2021a) '50 mb Zonal Wind Index.' Available at https://www.cpc.ncep.noaa.gov/data/indices/qbo.u50.index [Accessed 9 June 2021].

NOAA (National Oceanic and Atmospheric Administration) (2021b) 'Southern Oscillation Index.' Available at https://www.cpc.ncep.noaa.gov/data/indices/soi [Accessed 9 June 2021].

Rao, J., Garfinkel, C. I., White, I. P., Schwartz, C. (2020) The Southern Hemisphere Minor Sudden Stratospheric Warming in September 2019 and its Predictions in S2S Models. *Journal of Geophysical Research: Atmospheres* **125**, e2020JD032723.

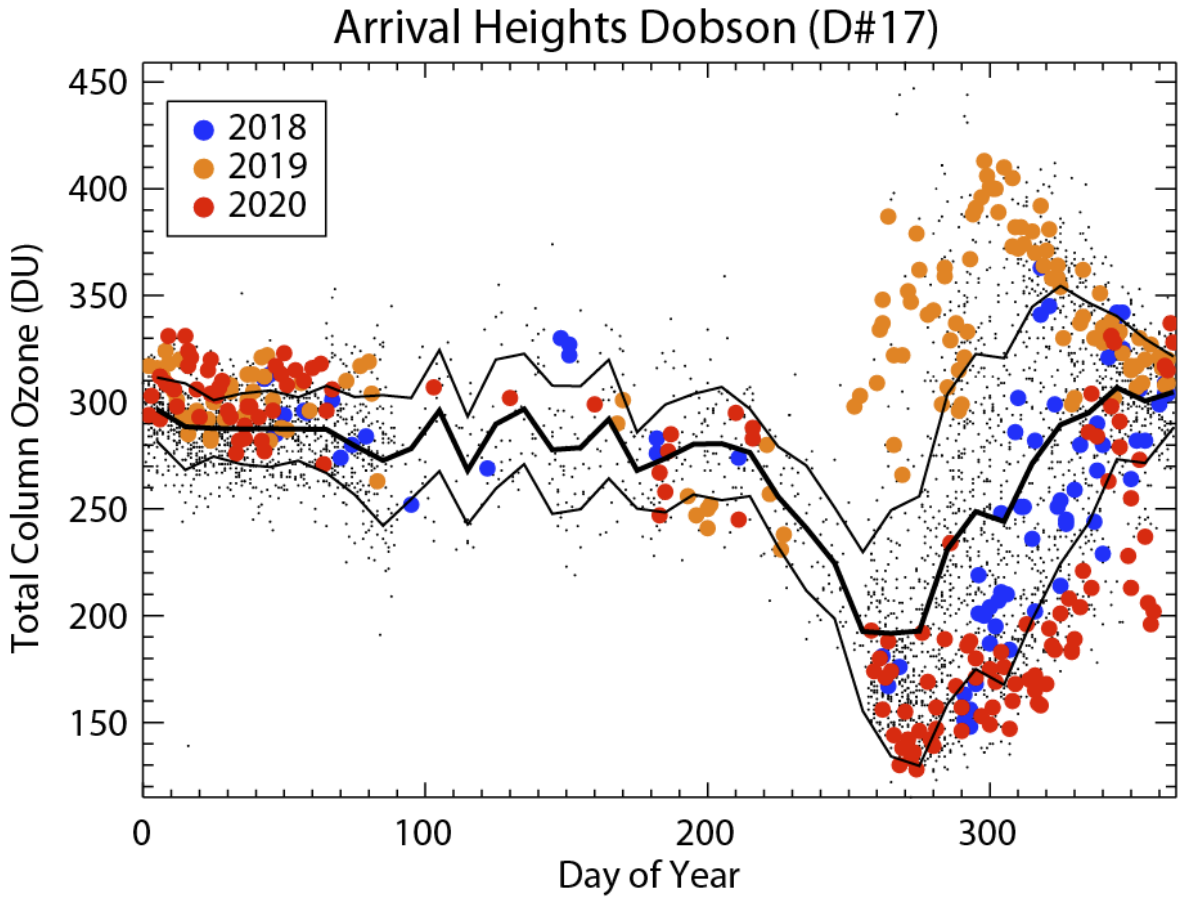

Fig. S1. Daily total ozone column abundance obtained from solar and lunar measurements with the Dobson spectrophotometer at Arrival Heights, Antarctica. Measurements for 2018, 2019 and 2020 are shown by blue, orange and red dots, respectively. Measurements in earlier years back to 1995 are shown as black dots. The solid line is the 10 day running mean over all years; the thin solid lines show the limits of one standard deviation from the mean.

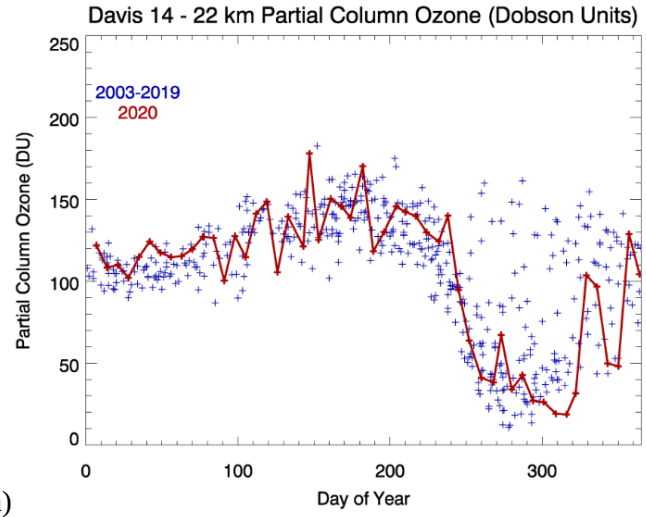

(a)

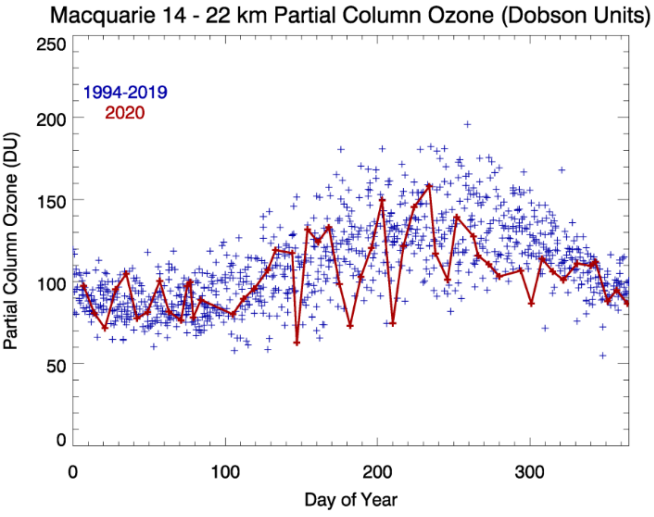

(b)

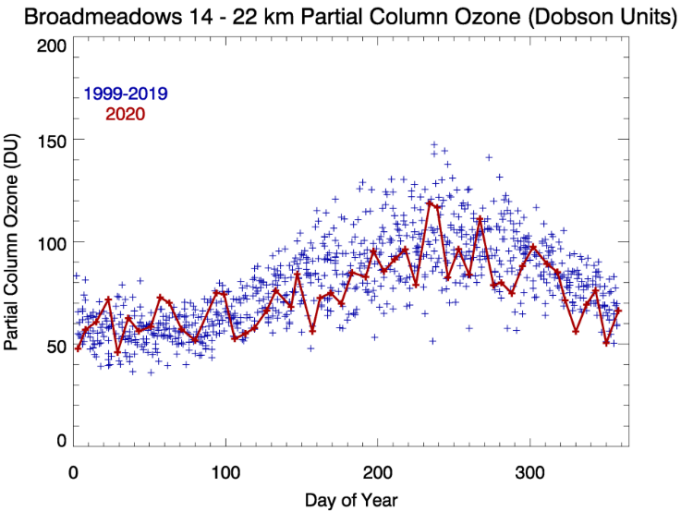

(c)

Fig. S2. Time series of partial column ozone over 14 – 22 km altitude from ozonesonde measurements at (a) Davis, (b) Macquarie Island and (c) Broadmeadows.

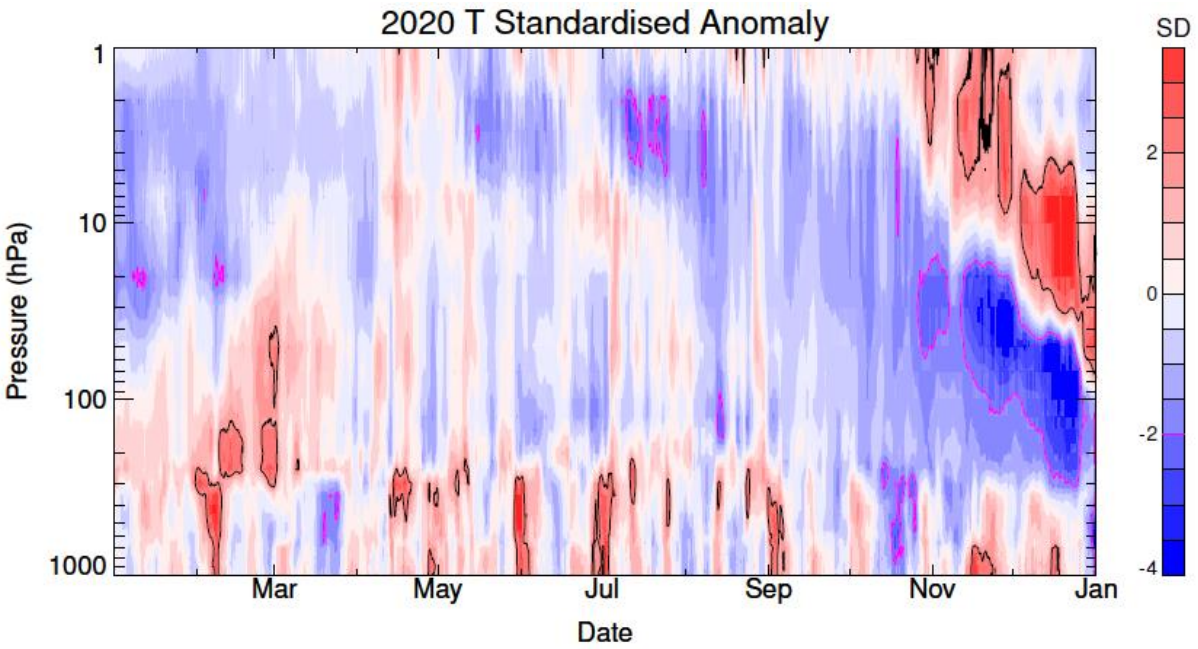

Fig. S3. Pressure-time section of the standardised temperature anomaly (in units of standard deviations, σ) obtained from ERA5 6-hourly data for the latitude range 70º S - 90º S for 2020. The anomaly is evaluated with respect to the 6-houly climatology at each pressure level over 1979 – 2019 and divided by the climatological standard deviation. The contours of -2 σ and + 2 σ are shown by the magenta and black contours, respectively.

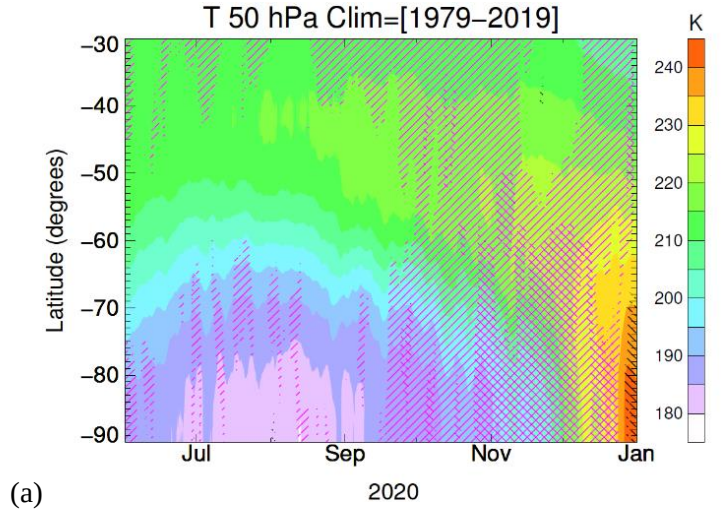

(a)

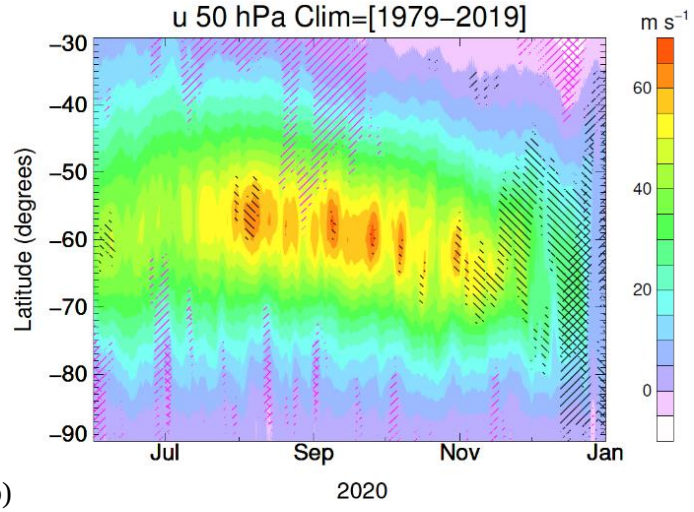

(b)

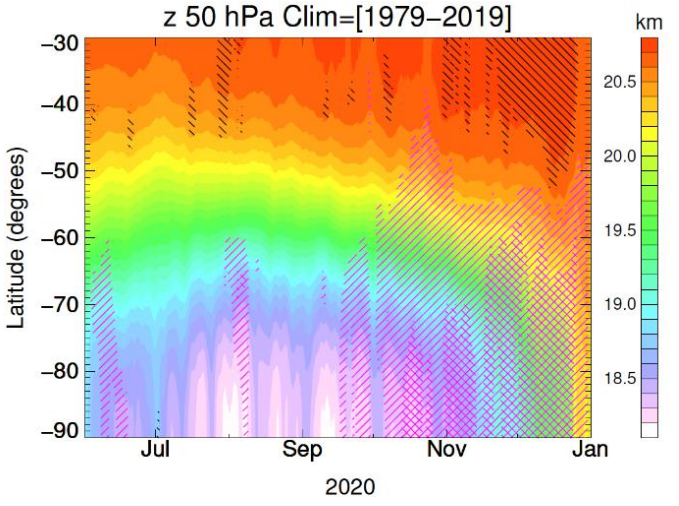

(c)

Fig. S4. Daily latitude-time sections at 50 hPa from ERA5 reanalysis. (a) Temperature. (b) Zonal wind. (c) Geopotential height. The anomalies are evaluated relative to the base period 1979 - 2019. Single diagonal hatching marks anomalies that are outside the inter-decile range (magenta: < 10^{th} percentile, black: >90^{th} percentile) of measurements prior to 2020. Values less than the daily climatological minimum or greater than the climatological daily maximum are shown by cross-hatched magenta and black lines, respectively.

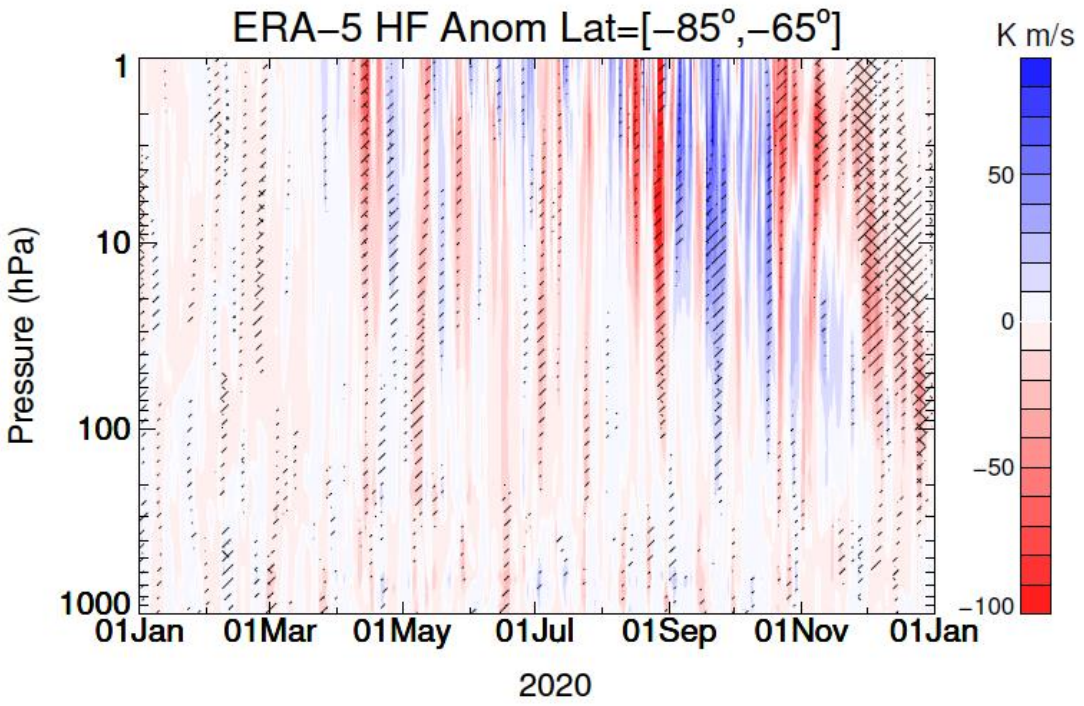

Fig. S5. Daily eddy heat flux anomaly as a function of pressure evaluated from the ERA5 reanalysis averaged between latitudes of 85°S-65°S for 2018 for 2020. Negative values (red colours) indicate enhanced poleward transport of heat. The base period of the daily climatology used to create the anomalies is 1979-2019. Single diagonal hatching marks anomalies outside the inter-decile range over the climatological period. Crossed diagonal hatching marks anomalies less than the minimum or greater than the maximum over the climatological period.

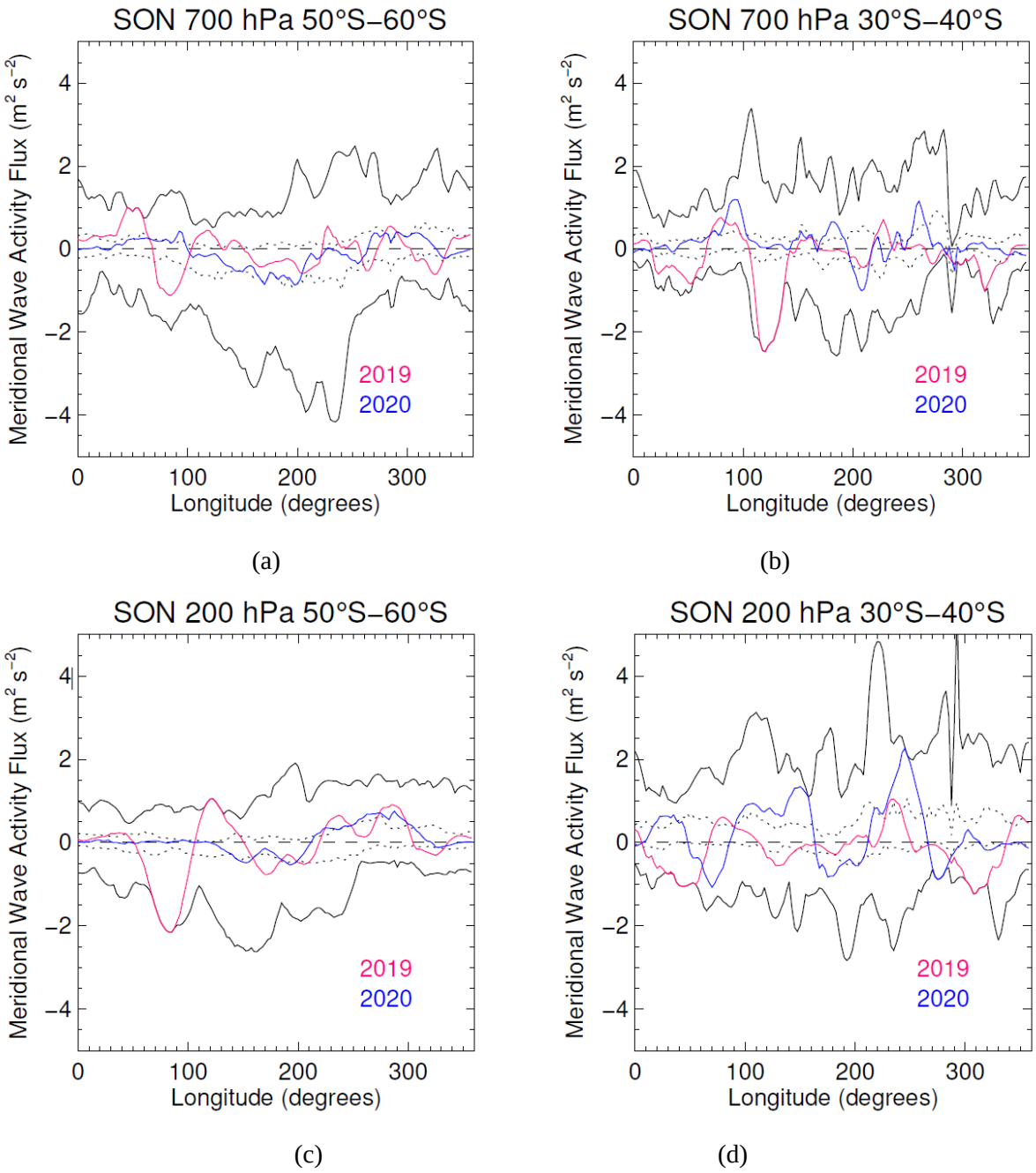

Fig. S6. Time series of the meridional component of the horizontal wave activity flux (See Section 2.4; units m^2 s^{-2}) averaged over September to November (SON) for two latitude bands and two pressure levels: (a) 700 hPa and 50º S - 60º S, (b) 700 hPa and 30º S - 40º S, (c) 200 hPa and 50º S - 60º S and (d) 200 hPa and 30º S - 40º S. Red and blue lines show time series for 2019 and 2020, respectively. The solid black lines show the maximum and minimum values over the years 1979-2020. The dotted black lines show the lower and upper quartile over 1979-2020.

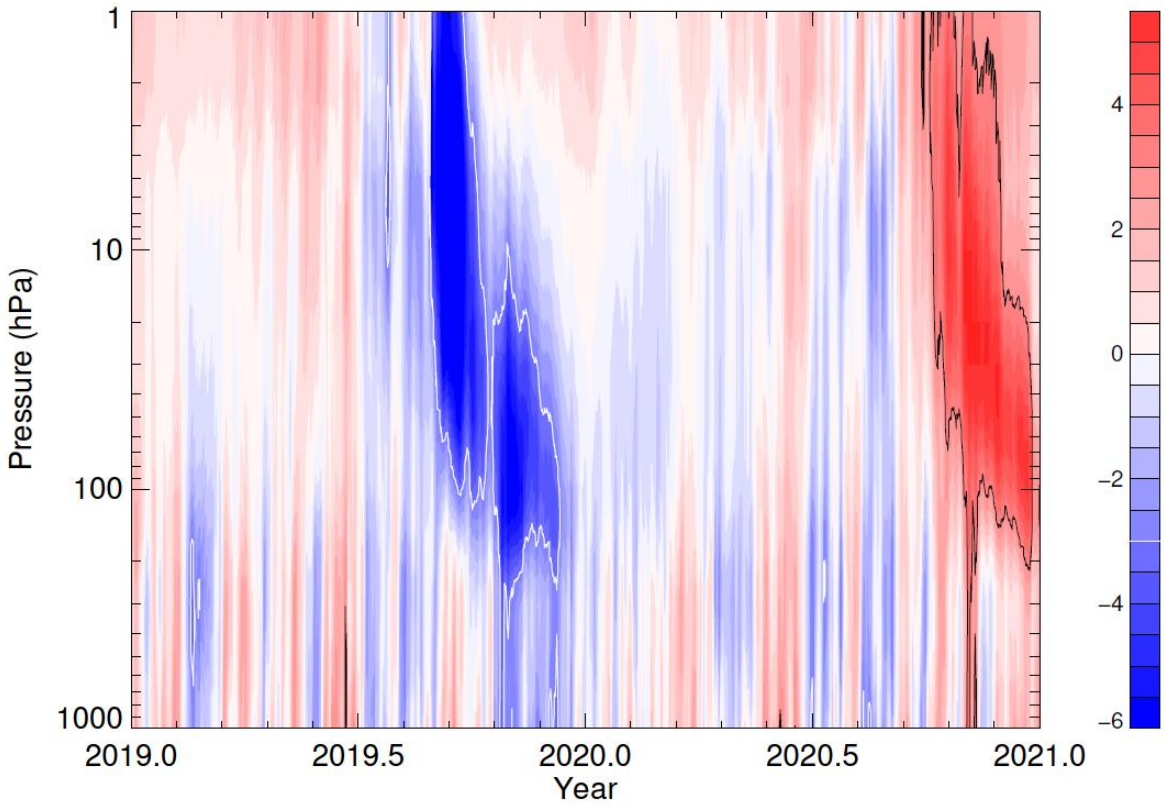

Fig. S7. Pressure-time section of the standardised Southern Annular Mode index (units: standard deviations, σ) from empirical orthogonal function analysis of 6-hourly ERA5 geopotential height data. The white and black contours are at -3 σ and +3 σ, respectively, over the 1980-2010 climatology.

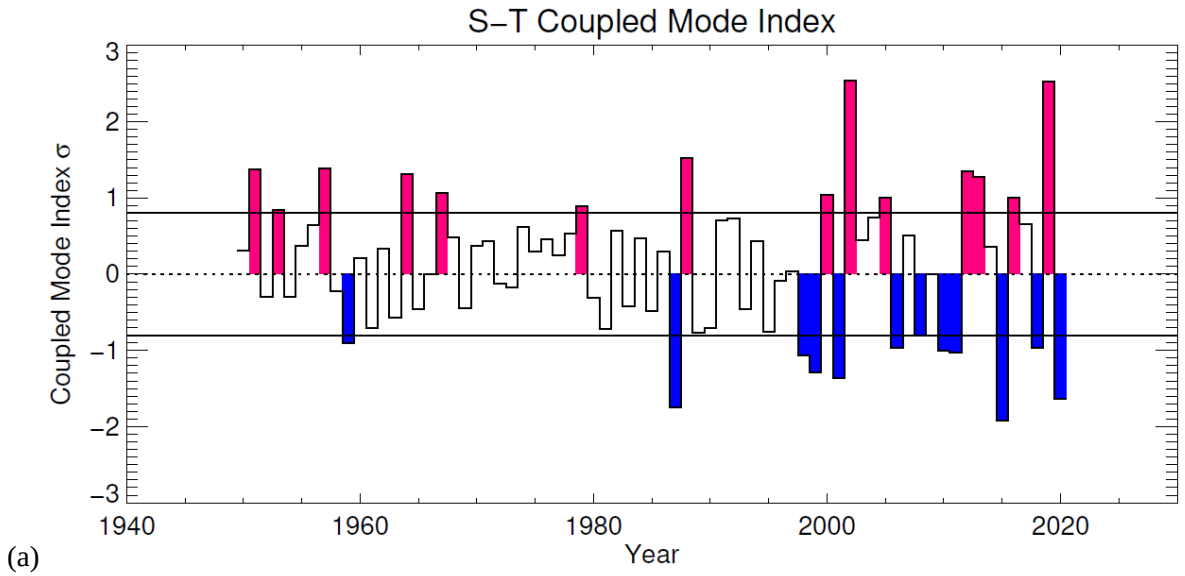

(a)

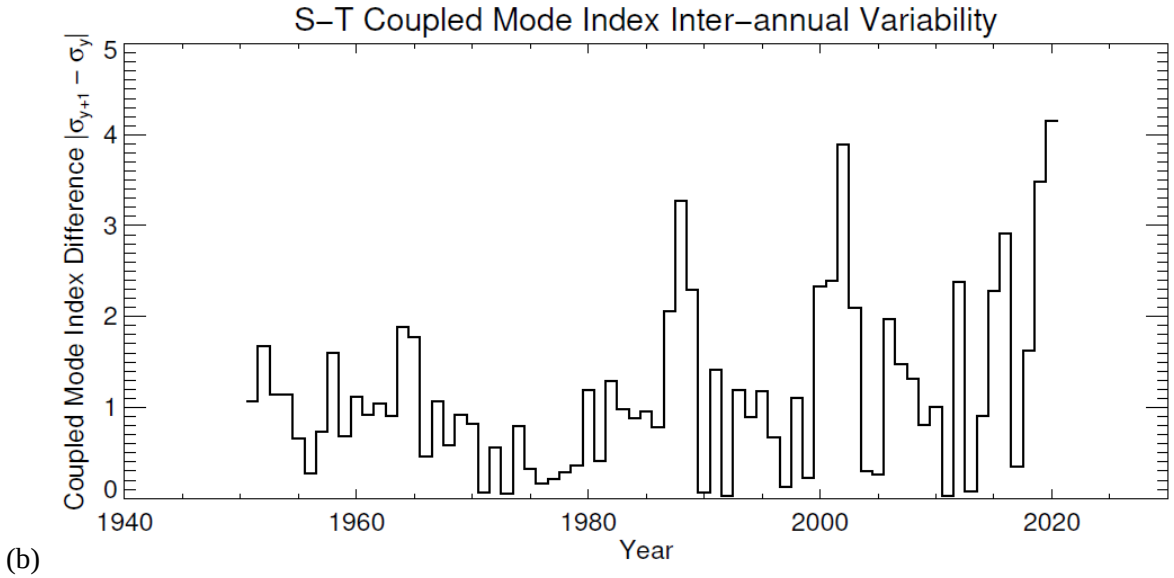

(b)

Fig. S8. (a) Time-series of annual standardised Stratosphere-Troposphere (S-T) coupled mode index from ERA5 analysis. The units are standard deviations (σ) and the base period used is 1979 – 2016. Strong and weak vortex years are shown as blue and red bars, respectively; neutral vortex years are not coloured. The thresholds of ± 0.8 σ are shown by solid horizontal lines. (b) Time series of the absolute value of the backward difference in the coupled mode index between adjacent years (subscript y = year number).